Crossover from self-trapped bound states to perturbative scattering in the Heisenberg-Kondo lattice model

Tanmoy Mondal¹ and Pinaki Majumdar²

¹ Harish-Chandra Research Institute (A CI of Homi Bhabha National Institute), Chhatnag Road, Jhusi, Allahabad 211019
² School of Arts and Sciences, Ahmedabad University, Navrangpura, Ahmedabad, India 380009
(Dated: October 29, 2025)

We map out the complete transport phase diagram of the ferromagnetic Heisenberg-Kondo lattice model in two dimensions. The model involves tight-binding electrons, with hopping t, coupled to classical spins with a coupling J', while the spins have a nearest neighbour coupling J between them. We work with a fixed, small, J/t, and study the temperature dependence of resistivity for varying electron density n, and coupling J'/t. Our magnetic configurations are generated by exact diagonalisation based Langevin dynamics, while the conductivity is computed using the Kubo formula on exact eigenstates. We work on lattices of size 20×20 and can access electron density down to $n \sim 0.01$. The electron system remains homogeneous either when the mean density is large or when the coupling J' is small. In these situations, the resistivity $\rho(T)$ displays a monotonic increase with temperature, and can be understood within a perturbative framework. However, at very low density, $n \lesssim 0.05$, strong coupling, $J'/t \gtrsim 1$, and for $T \sim T_c$, the electrons can locally polarise the magnetic state, create a trapping potential, and form a bound state in it. The resistivity associated with this polaronic phase is distinctly non-monotonic, with a peak near T_c . We establish the boundary that separates the many body polaronic window from traditional scattering and extract a universal form for the resistivity in the scattering regime. We suggest the origin of the 'excess resistivity' in the polaronic regime in terms of an increasing fraction of localised states as the temperature tends to T_c . This pushes the mobility edge towards the chemical potential μ and results in enhanced scattering of momentum states near k_F . While our specific results are in two dimensions, the phenomenology that we uncover should be valid even in three dimensions.

I. INTRODUCTION

For non-disordered electrons coupled to a spin system that transits from a ferromagnet at T=0 to an essentially uncorrelated paramagnet at $T\gg T_c$ there are two aspects of the resistivity $\rho(T)$ that are obvious. First, the resistivity vanishes as the temperature $T\to 0$, and second, the resistivity saturates when $T\gg T_c$. The questions are in the details, for example about (i) the scattering rate when $T\ll T_c$, (ii) the saturation value of the resistivity when $T\gg T_c$, and, most importantly, (iii) the nature of $\rho(T)$ when $T\sim T_c$. While (i) and (ii) are relatively straightforward, since the magnetic state is known, (iii) is the most interesting since the magnetic state has non trivial spatial correlations, and, additionally, at strong electron-spin coupling and low electron density the electrons can self-trap into magnetic polarons [1–18].

The scattering regime has long been explored, most importantly by Fisher and Langer [19], and the polaronic regime has seen some work in the last two decades [20–29]. This paper aims to establish a comprehensive picture connecting the two. The difficulty of the problem arises from two sources. The first relates to the magnetic state. In the presence of electrons, the magnetic correlation between the spins is no longer governed only by the Heisenberg superexchange but also involves electron mediated interactions. This is well understood in the weak coupling RKKY limit [24, 30] but does not have a simple analytic form at stronger coupling. So, even if we knew the magnetic correlations and T_c of the Heisenberg ferromagnet, we do not generally know the magnetic state in the presence of electrons. The second problem is related to electronic

properties in the equilibrium magnetic configurations. If J' were small, we can just compute resistivity, etc, in low order perturbation theory. When $J'/t \gtrsim 1$, however, 'naive' perturbation theory does not work. At high density, multiple scattering becomes important, and at low density, polarons can form. Most materials involve $J'/t \gtrsim 1$, with metals having electron density $n \sim O(1)$ [31, 32] and doped semiconductors having $n \sim 10^{-3} - 10^{-2}$ [14–18]. We need to go well beyond a Fisher-Langer scheme.

To generate the magnetic state accurately, retaining the electronic effect on the spins, and the thermal fluctuations, we use a Langevin dynamics scheme that diagonalises the electron problem at every time step [34–36]. In terms of accessing equilibrium configurations, this approach is equivalent to exact diagonalisation based Monte Carlo [20, 37, 38], widely used in manganite like problems. After equilibration we compute the conductivity by using the exact electronic eigenstates computed on the magnetic backgrounds. Using a parallelised algorithm that scales as N^2 , where N is the system size, we can access system size $\sim 20 \times 20$ within a reasonable time. The method can handle arbitrary J^\prime/t and temperature, and can access electron density down to ~ 0.01 - necessary for polaron physics.

While the crossover from a polaronic regime to a scattering dominated regime leaves its imprint on several measurables, e.g, optical conductivity, resistance noise, and muon scattering, in this paper, we focus only on the resistivity since it is the easiest to measure. Our main results are the following.

1. Using the electronic inverse participation ratio (IPR) and the resistivity, we establish a boundary in the $n-J^\prime/t$ plane that separates the polaronic window from the scattering dominated transport regime. Polarons require a critical coupling $J^\prime > J_c^\prime(n)$, shown in Fig.1. We also establish the thermal

window around T_c over which polaronic signatures exist.

- 2. Even at low densities relevant for polarons, the temperature associated with the emergence of ferromagnetic correlations strongly depends on n and J', since we are in a regime $J' \gg J$. We extract this temperature $T_c(n, J')$, which acts as the normalising scale in our resistivity.
- 3. We observe and explain a rough 'universal' form for the resistivity $\rho(T,n,J')$ away from the polaronic regime. This is exact both at weak and strong coupling and interpolates in between. This allows us to collapse the metallic resistivity to a form $\rho(T) = \rho_m(T) = \rho_\infty f(T/T_c)$, where ρ_∞ is the high T value, with a physically transparent n and J' dependence, and f is a normalised function.
- 4. In the polaronic window $\rho(T)$ strongly deviates from the metallic form $\rho_m(T)$ near T_c . The overall scale of the 'excess resistivity' near T_c , $\delta\rho(T)=\rho(T)-\rho_m(T)$, is set by ρ_∞ . We explain it's unusual temperature dependence, with a $d\rho/dT<0$ window, from the behaviour of the electronic lifetime as the polaronic mobility edge approaches the chemical potential μ .

The paper is organised as follows. In the next section, we briefly outline our computational strategy. Following that, successive sections discuss the transport phase diagram, the magnetisation and T_c , the resistivity, and the nature of electronic eigenstates. We end with a discussion of the scattering rate extracted from the single particle spectral function, and its correlation with the resistivity.

II. MODEL AND METHOD

We consider a square lattice with a spin \mathbf{S}_i , of unit magnitude, at each site, exchange coupled to the nearest neighbours by a coupling J. The spins are additionally coupled locally to electrons via a coupling J', and the electrons hop between nearest neighbour sites with an amplitude t.

$$H = H_{el} + H_{el-sp} + H_{sp}$$
$$= -t \sum_{\langle ij \rangle}^{\sigma} c_{i\sigma}^{\dagger} c_{j\sigma} - J' \sum_{i} \mathbf{S}_{i} . \vec{\sigma}_{i} - J \sum_{\langle ij \rangle} \mathbf{S}_{i} . \mathbf{S}_{j} \quad (1)$$

We set t=1 and J/t=0.1. In 3D, the classical Heisenberg model has a $T_c\sim 1.5J$. Our electron number is N_{el} , lattice size $N=L^2$, and electron density $n=N_{el}/N$. We vary the density in the range 1-12%.

In 2D, there is no genuine long-range order at $T \neq 0$, but on any finite $L \times L$ lattice there is a 'correlation temperature' $T_{corr}(L)$ where the magnetisation rises sharply as the temperature is lowered. It is known that $T_{corr} \sim 1/log(L)$ [39] for the 2D Heisenberg model. Our intent is to establish (i) the variation of the T_{corr} scale with n and J', staying at L=20, and (ii) the correlation between the magnetic and electronic state. These can be established, and spatial correlations visualised readily, in reasonably large 2D lattices. With this in mind, for notational simplicity we will just denote the correlation temperature $T_{corr}(L)$ by T_c .

At finite J' and n the effective magnetic model that determines the spin configurations is not simply H_{sp} but has cor-

rections coming from the electrons. Done exactly, the effective magnetic Hamiltonian is:

$$H_{sp}^{eff} = H_{sp} - \frac{1}{\beta} log[Tr \ e^{-\beta(H_{el} + H_{el-sp})}]$$
 (2)

where the trace is over electronic states in a given spin background. There are several ways to proceed from here. If J' were moderate we can extract the $O(J'^2)$ correction to H_{sp} in the form of a RKKY term. At even larger J', one can diagonalise $H_{el} + H_{el-sp}$ for each spin configuration and add the configuration dependent electronic free energy to H_{sp} Given this principle, one can use either Monte Carlo, or computing the "update cost" via diagonalization (an expensive process) or use H_{sp}^{eff} to generate an effective torque driving the spin dynamics. We use the second approach, detailed below, in the form of a Langevin equation, where the spins are subject to a systematic torque arising from H_{sp}^{eff} and a stochastic torque proportional to k_BT . This approach affords access to equilibrium spin configurations as well as the spin dynamics.

The Langevin equation governing the evolution of spins is given by:

$$\frac{d\mathbf{S}_{i}}{dt} = \mathbf{S}_{i} \times (\mathbf{T}_{i} + \mathbf{h}_{i}) - \gamma \mathbf{S}_{i} \times (\mathbf{S}_{i} \times \mathbf{T}_{i})$$

$$\mathbf{T}_{i} = -\frac{\partial H}{\partial \mathbf{S}_{i}} = -J' \langle \vec{\sigma}_{i} \rangle - J \sum_{\langle j \rangle} \mathbf{S}_{j}$$

$$\langle h_{i\alpha} \rangle = 0, \quad \langle h_{i\alpha}(t)h_{j\beta}(t') \rangle = 2\gamma k_{B} T \delta_{ij} \delta_{\alpha\beta} \delta(t - t') (3)$$

Here \mathbf{T}_i is the effective torque acting on the spin at the i-th site, γ is a damping constant set to 0.1t, and \mathbf{h}_i is a thermal noise satisfying the fluctuation-dissipation theorem. $\langle \vec{\sigma}_i \rangle$ represents the expectation of $\vec{\sigma}_i$ taken over the the instantaneous ground state of the electron in the spin configuration of the previous time step.

The primary indicators that we extract from our data are: (i) The instantaneous electron density: $n_i^{\alpha} = \sum_n |\psi_{i,n}^{\alpha}|^2$, where α is a spin configuration index and ψ_n is the eigenvector corresponding to the eigenvalue ϵ_n , obtained by diagonalising the electronic part of the Hamiltonian over spin configurations $\{\alpha\}$. The sum runs over the number of occupied states

(ii) We calculate the optical conductivity $\sigma(\omega)$ at low frequency to estimate the d.c conductivity. For a given spin background:

$$\sigma(\omega) = \frac{A}{N} \sum_{m,n} (f_n - f_m) \frac{|j_{mn}|^2}{\epsilon_m - \epsilon_n} \delta(\omega - (\epsilon_n - \epsilon_m))$$

The constant $A=(\pi e^2)/\hbar$. The matrix element $j_{mn}=\langle \psi_m|j_x|\psi_n\rangle$, and the current operator in the tight binding model is $j_x=ita_0e\sum_{i,\sigma}(c^\dagger_{i+xa_0,\sigma}c_{i,\sigma}-h.c)$. The ψ_m etc are single particle eigenstates, for a given spin configuration and ϵ_m,ϵ_n , etc are the corresponding eigenvalues. The f_m etc are Fermi factors. The d.c. conductivity in a given spin configuration α is σ_α

$$\sigma_{\alpha} = \frac{1}{\Delta\omega} \int_{0}^{\Delta\omega} d\omega \sigma_{\alpha}(\omega)$$

where $\Delta\omega$ is a small multiple of the average finite size gap in the spectrum. In our calculations, it is 0.05t. The d.c. resistivity is the inverse of the thermally averaged conductivity: $\rho = [\frac{1}{N_{\alpha}} \sum_{\alpha} \sigma_{\alpha}]^{-1}$. (iii) The inverse participation ratio (IPR) is $I_n^{\alpha} = \sum_i |\psi_{i,n}^{\alpha}|^4$. The inverse of this is an 'area' associated with the eigenstate, $A_{\alpha} = 1/I_{\alpha}$ (iv) The density of states is: $D_{\alpha}(\omega) = \sum_n \delta(\omega - \epsilon_n^{\alpha})$.

III. TRANSPORT CHARACTER NEAR T_c

Polaronic effects show up near T_c , where the magnetic system is most polarisable. Based on the electronic wavefunctions that arise on equilibrium magnetic configurations we can calculate the degree of localisation, which we present later in the paper. However, the simplest indicator of polaronic behaviour, as we argue later, is a peak in the resistivity near T_c . We will analyse this peak feature in the resistivity and correlate it to the spatial physics later, at the moment, we just show a phase diagram.

In Fig.1(a), the non polaronic regime is defined by an essentially homogeneous density and a monotonic temperature dependence in the resistivity. The low density strong coupling region, however, involves localised electronic wavefunctions near T_c (in a typical equilibrium configuration) and shows a peak in $\rho(T)$ near T_c . The phase boundary is defined by the vanishing of that peak as one moves out of the polaronic window.

The two main features in Fig.1(a) are the existence of (i) a minimum coupling $J'_{min} \sim 0.6t$ below which even single polarons do not form, and (ii) a maximum density, $n_{max} \sim 0.05$, above which polarons do not exist, however large the coupling. The presence of n_{max} suggests a minimum 'size' (or area A_{min}) to the polarons, set by $n_{max}A_{min}=1$. Given the value of n_{max} this area is ≈ 20 sites, suggesting a linear dimension to the polaron ~ 4 lattice spacings.

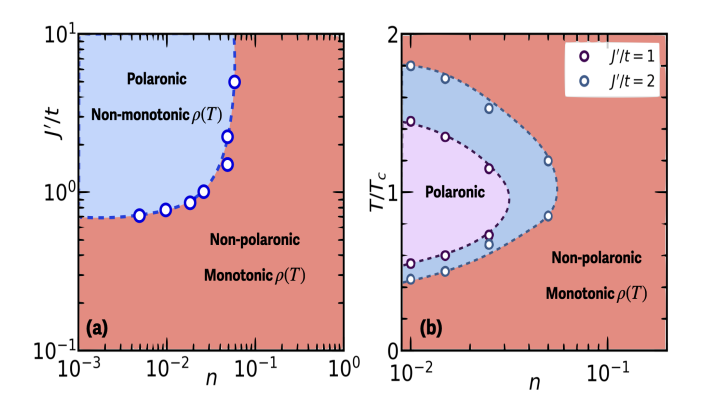


FIG. 1. Transport phase diagram. (a) The polaronic and non polaronic windows in the $n-J^\prime$ plane. In the non polaronic window, the resistivity $\rho(T)$ has a monotonic rise through T_c to a saturated high T behaviour. In the polaronic regime, there is a peak in the resistivity around T_c . This peak feature correlates with enhanced localisation of electronic states around T_c . (b) The temperature window over which polaronic effects are visible, identified through the resistivity.

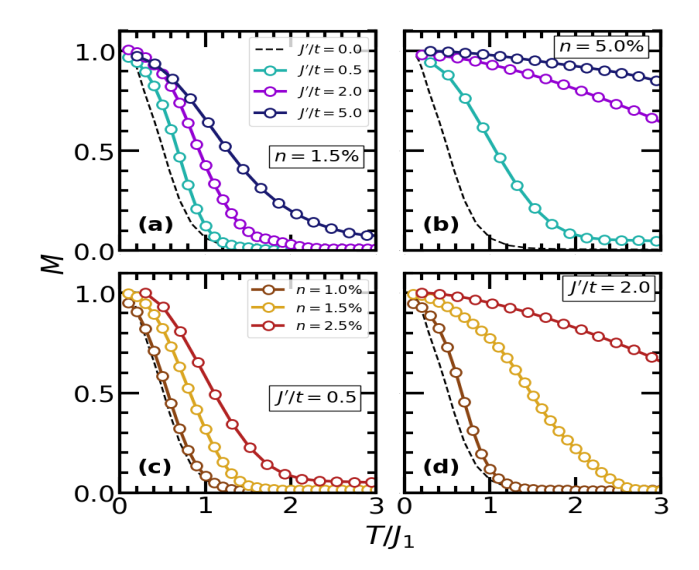


FIG. 2. Temperature dependence of magnetisation for different n and J'. (a)-(b) Variation of J' at low density n=1.5%, and somewhat larger density, n=5%, respectively. (c)-(d) Variation of n at J'/t=0.5 and 2.0. The highest density we have studied in this paper is $n\sim12\%$, that data is not shown here to keep the T scale manageable.

Fig.1(b) shows the temperature window, normalised by T_c , within which polaronic signatures are seen for a given n and J'. The low temperature state is fully polarised so electronic textures cannot form, while the $T\gg T_c$ state is entropy dominated, and again polaronic effects vanish. Between them is the region where $\rho(T)$ shows an 'excess resistivity', with respect to the expected background, and the occupied states show localisation. Fig.1(a)-(b) define the n-J'-T transport phase diagram of the model.

IV. MAGNETISATION AND T_c

In the presence of electrons, the magnetic state is no longer determined purely by the Heisenberg coupling. While the ground state continues to be ferromagnetic upto reasonably high density, the effective model describing the magnetism takes the following form at weak and strong coupling, respectively:

$$H_{eff} = -J \sum_{\langle ij \rangle} \mathbf{S}_{i}.\mathbf{S}_{j} + J'^{2} \sum_{i \neq j} \chi_{ij} \mathbf{S}_{i}.\mathbf{S}_{j}, \qquad J'/t \lesssim 1$$

$$H_{eff} = -J \sum_{\langle ij \rangle} \mathbf{S}_{i}.\mathbf{S}_{j} - tf(n) \sum_{\langle ij \rangle} \sqrt{\frac{1 + \mathbf{S}_{i}.\mathbf{S}_{j}}{2}}, \quad J'/t \gg 1$$

f(n) is a density dependence that vanishes as $n \to 0$ and is maximum at n=0.5. The corrections above are, respectively, the RKKY interaction and (an approximate form of) the double exchange interaction. They both enhance the ferromagnetic exchange compared to J. We are working in a regime where $J \ll t$ so the effective exchange, at a given n, would rise as J'^2 from the Heisenberg limit and saturate to a value $\propto t$ at large J'.

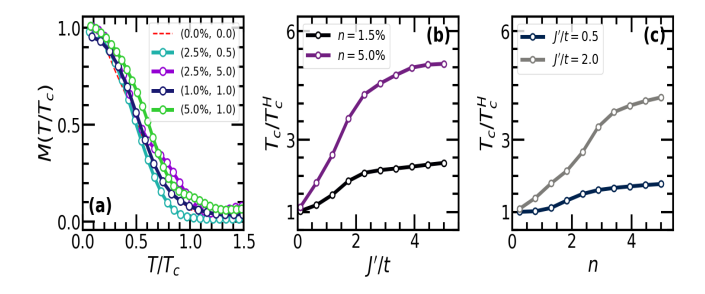


FIG. 3. Scaling of the magnetisation, and T_c scales. (a) Plot of $m(T/T_c)$ to check that the overall behaviour has a similar pattern independent of n and J'. The approximate collapse will allow us to encode magnetic information only in terms of T_c . The legend indicates (n, J'/t) values corresponding to each curve. (b) $T_c(J')$ for two values of n. (c) $T_c(n)$ for two values of J'.

As we have mentioned before, there is no true T_c in 2D but only a size depedent correlation temperature $T_{corr}(L)$, which we denote as T_c for convenience. Fig.2(a)-(b) show the J' dependence of the magnetisation m(T) at densities n = 1.5%and n = 5%, respectively. The dotted curve is the reference Heisenberg result, and the temperature is scaled with respect to the Heisenberg exchange J. Apart from the obvious increase in T_c with J' in both cases, and the larger increase at higher electron density, we note that even at a low density like 1.5\% a coupling J' = 2t (typical of the polaronic phase) almost doubles the T_c ! The doubling is of course because we have taken a low value, J = 0.1t. Superexchange couplings are typically a few percent of t, while electron-spin couplings are O(t), so even a dilute electron system will affect the T_c noticeably. Thankfully, it does not change the nature of the ground state.

Since we will scale all temperatures with respect to T_c we wanted to check that the magnetisation profile has a reasonably common look when scaled by T_c , i.e, $m(T,n,J') \approx m(T/T_c(n,J'))$. Fig.3(a) shows this 'collapse'. This is hardly surprising since the m(T) is constrained for all n and J' by m=1 at T=0 and $m\to 0$ for $T\gg T_c$ (on a finite size) and the magnetic model has the same symmetry throughout. The plot shows data for a combination of n and J'.

Fig.3(b) shows the increase of T_c with respect to the Heisenberg result at two values of n, as J' is changed. They have a small J'^2 window, hard to access on our lattice size (where the smallest J' is 0.5t), and both curves saturate for $J'/t \gtrsim 4$. The 'double exchange' limit, it seems, is quickly reached. The actual enhancement of T_c in the large J' limit is $\sim 2.5T_c^H$ at n=1.5% and $\sim 5T_c^H$ at n=5%. Fig.3(c) shows the n dependence of T_c for two values of J'.

V. RESISTIVITY

Our main focus in this paper is the resistivity, and we would like to explore the temperature dependence at various n and J'. From that, we want to infer the phase diagram of Fig.1.

It is best to think in terms of four scans of the n-J' plane. The simplest would be $J'/t\lesssim 1$ where the magnetic state

is only weakly affected by the electrons and the scattering of electrons from the spin background can be captured with lowest order perturbation theory in J'. Fig.4(a) shows the result for J' = 0.5t and four values of n. In all cases $\rho(T)$ vanishes as expected as $T \to 0$, where the magnetic state is fully polarised and there is no scattering, and tend to a n dependent constant for $T \gg T_c$, where the electrons scatter from uncorrelated spin disorder. Since J'/t is small one expects that the $\rho(T)$ would be decided by a Drude form: $\sigma(T) \sim ne^2 \tau/m$, i.e, $\rho(T) \propto \Gamma(T)/n$, where the scattering rate $\Gamma = 1/\tau \propto J'^2$ at weak coupling. The T dependence of Γ was proposed by Fisher and Langer long back, we will discuss this later. At this moment we just note that the high T values in Fig.4(a) indeed vary as 1/n. We have also checked that even at low n the spatial density n_i , in individual magnetic configurations, remains essentially homogeneous at all T. There are no polaronic effects.

We now want to check the J' dependence, at reasonably high density where we do not expect polarons. Fig.4(b) shows results at n=12.5% for varying J' - all the way from 0.5t to 5t. The $\rho(T)$ looks similar to what we saw in panel (a), except the high T values are now functions of J'. Note that the high T values do not increase as J'^2 at large J'. The next two panels, (c) and (d), would bring in T dependence quite unlike what we see in (a) and (b).

Panel (c) shows the effect of increasing coupling at a low density n=1.5%. At J'=0.5t, the lowest curve, the resis-

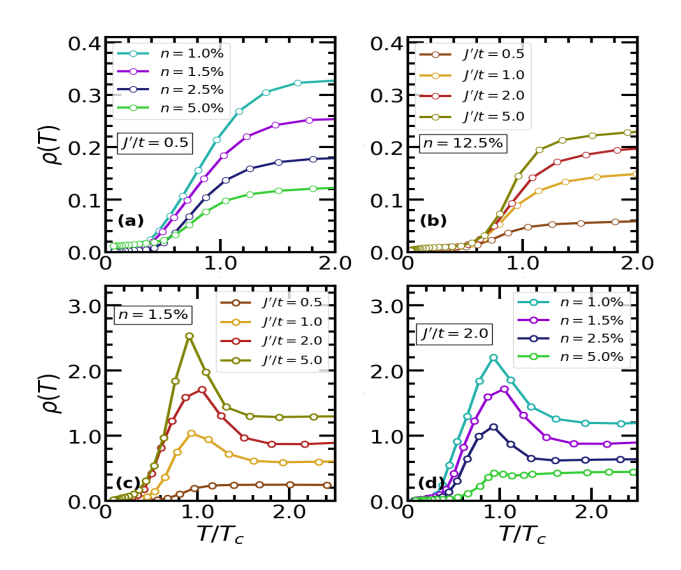


FIG. 4. Resistivity $\rho(T)$. (a) Density variation at weak coupling, J'=0.5t. Note the monotonic T dependence of $\rho(T)$ and the increasing high T saturation value as n is lowered. (b) 'High density' n=12.5% case for varying J'. The temperature dependence shares a similarity with (a). (c) Increasing J' at low density n=1.5%. While the weak coupling resistivity is monotonic, for $J'\geq t$ the resistivity is distinctly non monotonic, with a peak near T_c . The high T value also increases with J'. Essentially, at low n one enters an unusual transport regime with increasing J'. Finally, (d) Increasing density, starting from low n, in the strong coupling regime. Here, the peak structure weakens with increasing n and almost vanishes for n=5%.

tivity is monotonic. The three other curves, for J'=t and above, shows a clearly non monotonic behaviour. There is an 'excess resistivity', with respect to a hypothetical monotonic background (see later), for T around T_c .

Panel (d) shows density increase at J'=2t. It has the n=1.5%, J'=2t data in common with panel (c). If we decrease n with respect to n=1.5% we find an enhanced peak in $\rho(T)$, and a higher high temperature value. If we increase n we find a weakening of the peak and a move towards a more 'normal' resistivity.

Let us try to make some sense of the resistivity results. While the weak coupling resistivity is expected to have an overall scale varying as $(1/n)J'^2$, as J' increases the quadratic dependence on J' would be increasingly inaccurate. The scattering rate would pick up contributions of order J'^4 , J'^6 from multiple scattering. Remarkably, we know the answer for $J'/t \to \infty$, the 'double exchange' limit, where J' gets absorbed in the chemical potential and one obtains a hopping disorder model (see Discussion) whose overall scale is t [20, 40, 41].

Based on this, the weak coupling resistivity for $T\gg T_c$ would be $\propto (1/n)J'^2/t$, while at strong coupling the $T\gg T_c$ resistivity should be $\propto (1/n)t$. The scattering rates could have a density dependence via the density of states, but in 2D and low density the density of states is energy independent. We can try an interpolative form for the high temperature resistivity $\rho(T\gg T_c)\equiv \rho_\infty$, given by: $\rho_\infty=(A/n)(J'^2/t)/[1+\alpha(J'^2/t^2)]$.

For $J'/t \to 0$ this gives $\rho_\infty \sim (\frac{1}{n})J'^2/t$, and for $J'/t \to \infty$ it gives $\rho_\infty \sim (\frac{1}{n})t$, satisfying both the limits. This raises three questions: (i) does this fit our grid of n-J' data? (ii) after scaling $\rho(T)$ by ρ_∞ we get a normalised ρ that varies

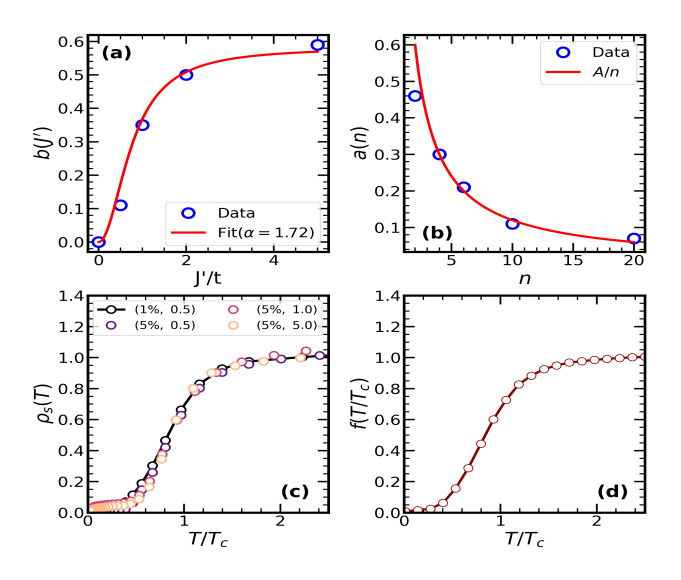


FIG. 5. Fitting functions for the resistivity $\rho(T)$. (a) The J' dependence fitted to a form ${J'}^2/(1+\alpha J'^2)$ shows a reasonable fit with $\alpha=1.72$ for all n. (b) A fit to the n dependent prefactor to a form A/n in the window 0-10%, gives $A\sim1.2$. (c) The scaled resistivity $\rho(T/T_c)/\rho_\infty$ for some combinations of n and J'. (d) The best fit $f(T/T_c)$ to the normalised T dependence shown in (c).

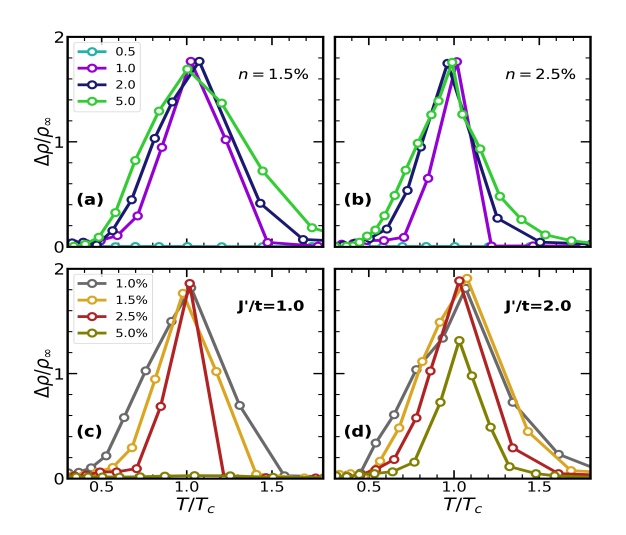


FIG. 6. The normalised 'excess resistivity' defined by $\delta\rho(T/T_c)=(\rho(T/T_c)-\rho_{\infty}f(T/T_c))/\rho_{\infty}$. (a)-(b) shows J' variation at two n, while (c)-(d) show n variation at two J'. All these points are in the polaronic window in Fig.1. Notice that the overall magnitude of $\delta\rho$ is $\lesssim 1$, indicating that the overall magnitude of $\rho(T)$ is set by ρ_{∞} - however deep one may be in the polaronic regime. While the temperature window over which $\delta\rho$ is non zero seems to be similar in all cases, $\approx 0.5T_c-2T_c$, the windows are somewhat larger at small n and large J'.

from 0-1 with T - is this an universal function of T/T_c and not dependent separately on J' and n? (iii) what is the value of α ? If the answers to (i) and (ii) are in the affirmative then we have a complete characterisation of at least the non polaronic window, and can examine the polaronic regime with respect to this reference.

We try out the fitting. First, at a fixed density, n=12.5% we fit ρ_{∞} to the form $(J'^2/t)/(1+\alpha(J'^2/t^2))$. The quality of the fit is shown in Fig.5(a), and gives $\alpha=1.72$. When we try this at other n, putting in the prefactor 1/n we find the α to be independent of n. On the whole ρ_{∞} can be fitted to the form:

$$\rho_{\infty} = \left(\frac{A}{n}\right) \frac{J'^2/t}{(1 + \alpha(J'^2/t^2))}$$

with $A \approx 1.2$, $\alpha \approx 1.72$.

What about the actual temperature dependence? We plot the scaled resistivity $f(T) = \rho(T)/\rho_{\infty}$ for several n and J' combinations in Fig.5(d) with respect to T/T_c . Given the finite size issues and uncertainty in T_c determination, we think one can reasonably argue for "collapse" to a single characteristic. It is possible that detailed calculations on the Heisenberg-Kondo model in 3D in the tractable $J'/t \ll 1$ and $J'/\gg 1$ limits will reveal small differences between the scaled resistivity, but the larger characterisation of the metallic phase should survive. So $\rho(T,J,n)=\rho_{\infty}(J,n)f(T/T_c)$.

What if we test out this function in the polaronic regime, now that we know it's n and J' dependence? The fit works well at low and high T but we obtain an excess resistivity

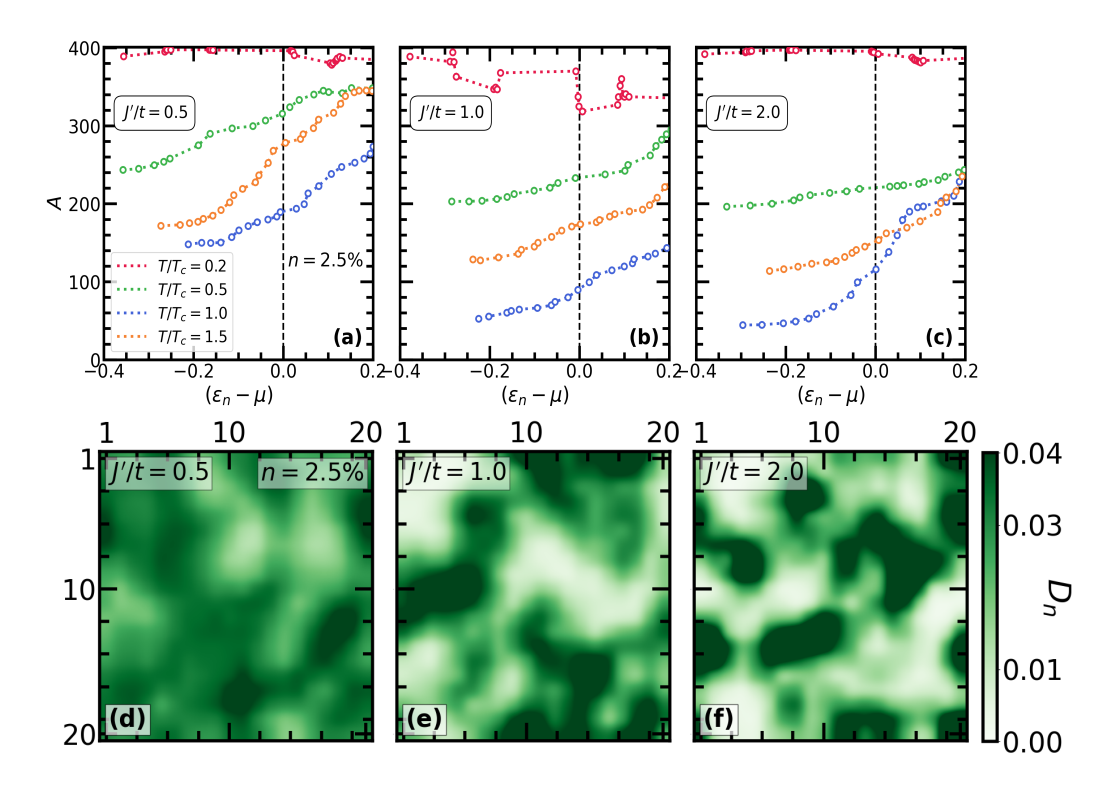


FIG. 7. The area A associated with an eigenstate in typical magnetic configurations at different T/T_c , for n=2.5% and J'/t=0.5, 1.0, 2.0. (a) A_n is \sim system size at $T=0.2T_c$ for all n. With $T\to T_c$ the A_n for the occupied states decrease quickly, but even at the lowest, they are ~ 150 . Beyond T_c the A_n rise again. (b) Same density but J'=t. Again $A_n\sim 400$ at low T, but at T_c the occupied states have A_n ranging from 50-100. The density field, as we see later, has a textured pattern, but the localisation near T_c is still weak, $N_{cl}A_{av}>N$, with $A_{av}\sim 75$. For T increasing beyond T_c the A_n increase. (c) Now J'=2t. In the same trend as in (b), we now have even smaller values of A_n for the occupied states at T_c , but still $N_{cl}A_{av}>N$ - no well separated polarons. At n=2.5% we will need $A_{av}\sim 40$ for well localised polarons to exist.

around T_c , defined by

$$\delta\rho(T/T_c) = \frac{\rho(T/T_c) - \rho_{\infty}f(T/T_c)}{\rho_{\infty}}$$

This is shown in Fig.6. Panels (a)-(b) show the J' dependence at n=1.5% and 2.5%, respectively, while (c)-(d) show the n dependence at J'=t and J'=2t. The first observation is that the peak in $\delta\rho$ is always in the range 1.8-2.0, which means it scales with ρ_{∞} at that n and J'. The peak occurs around T_c , and the function is non zero in the interval $\sim 0.5T_c-2T_c$. Looked at closely the temperature window does have some variation with n and J', but for the moment let us focus on addressing the overall structure of $\delta\rho$. Does it arise from

- Localisation of states at the chemical potential as T increases towards T_c and progressive delocalisation thereafter? Or, is it related to
- An enhancement in the scattering rate of delocalised states at the chemical potential as T increases towards T_c , and its decrease thereafter?

This requires us to examine the eigenstates in typical magnetic configurations at various T for different combinations of n and J'.

VI. EIGENSTATES AND MOBILITY EDGE

The inverse participation ratio (IPR) is the standard measure of localisation of single particle states. We use the inverse of this object as a measure of the area covered by an eigenstate. Thus $A_n = [\sum_i |\psi_i^n|^4]^{-1}$, where we assume a normalised state. For a plane wave, we would have $\psi_i^n = 1/\sqrt{N}$, so A_n would be N, the number of lattice sites. Correspondingly, a state distributed uniformly over N_p sites will have $A=N_p$.

Fig.7 shows A_n for electronic eigenstates ψ_n from typical equilibrium spin configurations at four temperatures from $0.2T_c$ to $1.5T_c$. Panel (a) shows A_n at n=2.5% and J'=0.5t. Negative values of $\epsilon_n-\mu$ correspond to the occupied states (modulo Fermi function effects). At $T=0.2T_c$ where the magnetic state is essentially polarised the electrons see very little disorder, and $A\approx 400$ for all ϵ_n on our 20×20 lattice. With T increasing towards T_c , the A_n associated with the occupied states drop, reaching a minimum ~ 150 sites at T_c . The average A_{av} of A_n over the occupied states at this T is ~ 170 . This is too large for isolated polarons in a $N_{el}=10$ system, since $N_{el}\times A_{av}\sim 1700\gg 400$, the system size. We have also confirmed that the spatial density remains essentially uniform at T_c . With T increasing beyond T_c the A_n

increases. So, no polarons at this (n, J') point, at any T, consistent with the monotonic $\rho(T)$.

Panel (b) shows results at the same density but J'=t. All the A_n traces are systematically lower than the corresponding J'=0.5t case, but even here A_{av} at T_c is ~ 75 , with $N_{el}A_{av}>N$. We see an increasing tendency towards localisation but no well separated polarons yet. Panel (c), at J'=2t, shows a similar trend, with $A_{av}\sim 75$ at T_c , not small enough for isolated polarons. What we see in (b) and (c) are reasonably compact low energy states but as $\epsilon_n\to\mu$ there is a rapid increase in A_n . The states near μ , which will decide the d.c conductivity can be called weakly bound or strongly scattered at this system size.

We now focus on T_c and show a wider density variation at J'=2t. Fig.8 shows that at high density, n=12%, we have $A_n\sim 400$ even at T_c The A_n profile gets lowered systematically as n decreases. However, it is only for the lowest two plots, n=1% and 1.5%, that $N_{el}A_{av}\lesssim N$. When this product is $\lesssim 1$ we have a well localised polaronic phase.

Since the polarons are localised states, in contrast to the higher energy delocalised states, we now go through the exercise of identifying a 'mobility edge' ϵ_c in the density of states, at a given T. This is a risky venture since locating ϵ_c in a standard disordered system involves systematic increase in system size and locating which states have IPR O(1) (localised) versus IPR O(1/N) (delocalised). Given the computational cost of our basic calculation, we cannot do a significant size variation and arbitrarily set $A_n=60$ as cutoff for a localised state. We also checked what happens when we set a cutoff of 40 - the dashed line in Fig.9 shows this.

Fig.9 shows the mobility edge, using this criterion, for two densities, n=1% and n=2.5% and J'=1, at $T=T_c$. Panel (a) shows that ϵ_c remains below, but close to μ at n=2.5% while at n=1% it actually coincides with μ . Fig.10 will show how $\epsilon_c-\mu$ varies with temperature in a few cases.

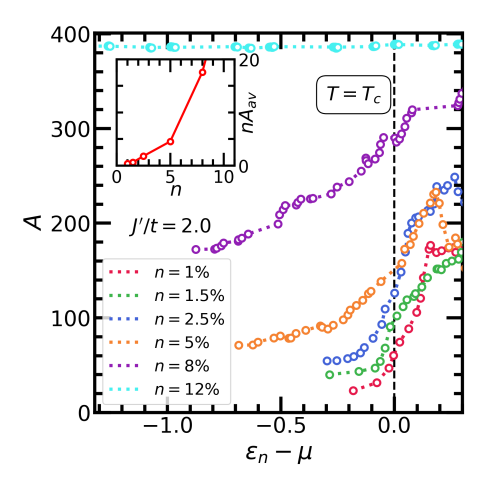


FIG. 8. The area A_n for several n at J'=2t and T_c . At the highest density, n=12%, all states remain delocalised. There is a suppression in the A_n for the occupied states as n decreases to 8% and 5%, but the A_{av} for the occupied states is still too large. For the lowest two n however the occupied states are sufficiently compact for the system to be characterised as polaronic.

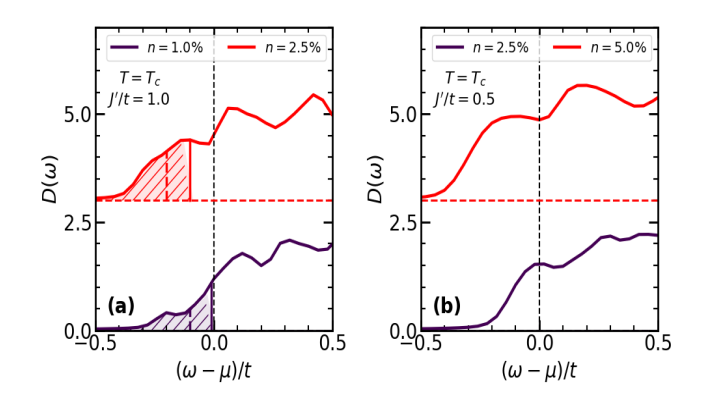


FIG. 9. The density of states, showing the 'mobility edge' separating the localised (shaded) states from the delocalised ones. (a) J'=t and n=1% and 2.5%, and $T=T_c$. At the higher n, the mobility edge remains below μ , while at the lower n, it almost coincides with μ . All this is assuming $A \leq 60$ as a localised state. (b) Same as (a) but now with J'=0.5t. There are no localised states and the mobility edge is at the band bottom.

Panel (b) shows the DOS for the same two densities but now at J'=0.5t and $T=T_c$. There are no localised states in this case and the mobility edge is basically at the lower edge of the band.

With all the uncertainty about the accurate location of ϵ_c in the DOS, we can still track its T dependence using the criteria chosen. Fig.10 shows $\epsilon_c(T) - \mu(T)$ for densities $n=1,\ 2.5,\ 5\%$ at J'=2t. In all three cases $\epsilon_c-\mu$ is 'flat' for $T<0.5T_c$, remaining pinned at the lower edge of the band. Beyond $T\sim0.5T_c$ it starts rising, has a peak near T_c , and drops back again. At the two higher densities ϵ_c approaches the chemical potential and then recedes at higher T,

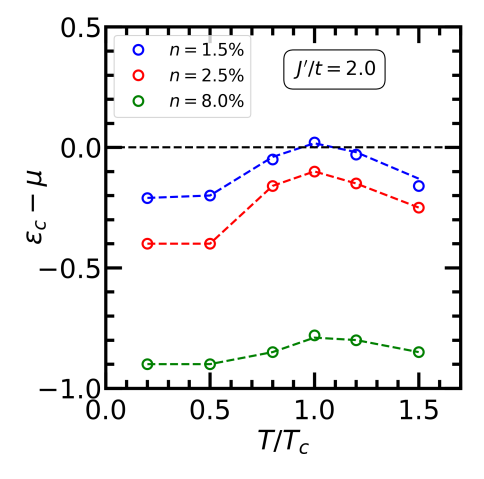


FIG. 10. The temperature dependence of the mobility edge, with respect to the chemical potential, at J'=2t and three values of n. In all cases ϵ_c starts at the band bottom at T=0 and essentially stays there for $T\lesssim 0.5T_c$. After that, it rises, has a maximum near T_c , and drops again. For n=1%, and with our definition of localised states, the mobility edge does cross μ for n=1%, but for the higher densities it approaches μ but never crosses.

while at n=1% it actually crosses μ and falls below again as T crosses $\sim 1.5T_c$.

This result is important in creating an understanding of the excess resistivity, with respect to perturbative scattering, that one sees in the polaronic regime. It seems in general that a 'mobility gap', $\epsilon_c - \mu > 0$, over a certain temperature window around T_c , is not the generic scenario behind the non monotonic resistivity. States near μ have a spatial extent which are a fair fraction of system size. The non monotonicity in the area $A(\mu)$ with T and now the non monotonicity of $\epsilon_c - \mu$ correlates with the non monotonicity of $\rho(T)$, but we want a more quantitative connection. With that in mind, we opted to compute the electron spectral function $A_{\sigma}(\mathbf{k},\omega)$, for the small \mathbf{k} values in the low density window, and check the scattering rate from its width.

VII. SINGLE PARTICLE SCATTERING RATE

The conductivity is determined by the current-current correlation in equilibrium magnetic configurations, and then thermally averaged. Within our model of electrons coupled to classical spins this can be written in terms of the 'unaveraged' Green's functions $G_{\sigma\sigma'}(\mathbf{k},\mathbf{k}',\omega)$. The spin and momentum off-diagonal components of G exist since the electrons can undergo spin-flip scattering from the magnetic background.

To get an estimate of the scattering rate we chose to compute the spectral function

$$A_{\sigma}(\mathbf{k},\omega) = -(\frac{1}{\pi})Im\big[G_{\sigma\sigma}(\mathbf{k},\mathbf{k},\omega)\big]$$

This can be related to the overlap of momentum eigenstates $|\mathbf{k},\sigma\rangle=c_{\mathbf{k},\sigma}^{\dagger}|0\rangle$ with the exact eigenstate $|n\rangle=a_{n}^{\dagger}|0\rangle$ of the electron in the magnetic background. Denoting $\langle n|\mathbf{k},\sigma\rangle=$

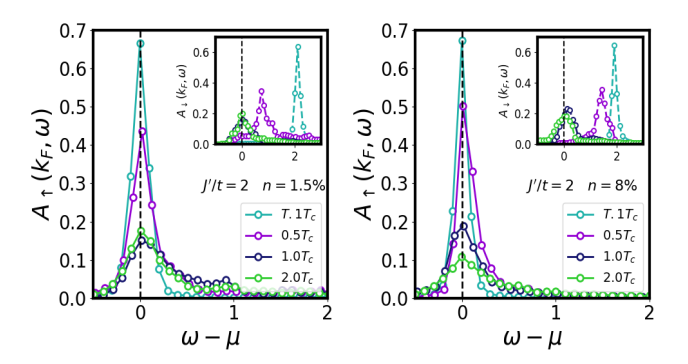


FIG. 11. Single particle spectral function $A_{\sigma}(k_F,\omega)$: We compute the spectral function using the exact eigenstates and eigenvalues in individual equilibrium spin configurations and then average thermally. (a) The main panel shows $A_{\sigma}(k_F,\omega)$ in the polaronic regime, with a non monotonic behaviour as a function of T. (b) Shows the result at the same J' but larger n, where no polarons exist, and the spectra broaden monotonically with increasing T. The insets show the spectra in the minority spin channel.

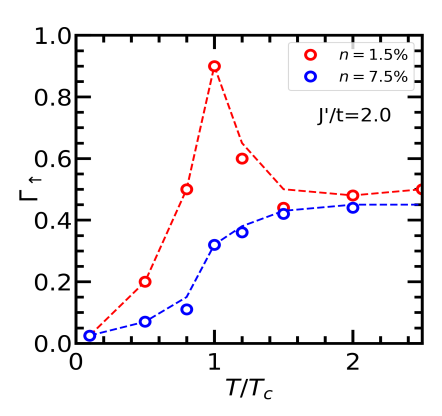


FIG. 12. Scattering rate in the polaronic and non polaronic regimes. We extract the half width of $A_{\uparrow}(k_F,\omega)$ and show it's temperature dependence in the polaronic n=1.5% and non polaronic n=7.5% cases. The prominent peak in the polaronic case correlates with the behaviour of the resistivity.

 $u_{\mathbf{k},\sigma}^n$, we have

$$A_{\sigma}(\mathbf{k},\omega) = \sum_{n} |u_{\mathbf{k},\sigma}^{n}|^{2} \delta(\omega - (\epsilon_{n} - \mu))$$

We know the eigenvalues and eigenfunctions in each equilibrium spin background and so can calculate A, and average it over thermal configurations at a given T.

The expression we had suggested earlier to model the background resistivity is based on leading order perturbation theory, and would work if the chemical potential is far from a mobility edge. However if ϵ_c approached μ the scattering rate Γ_σ would exceed the background value. Rather than attempt a complicated approximation for the Γ we chose to extract it directly from the width of the spectral function at $k \sim k_F$ (at the low n that we use the FS is circular).

Fig.11(a) shows $A_{\sigma}(\mathbf{k},\omega)$ in the polaronic phase, n=1.5% and J'=2t, at four temperatures. The main panel shows the spectra for spin up (majority) while the inset shows the result for spin down. At $T\ll T_c$ transport will be dominated by the up spin channel, while for $T>T_c$ the up and down spin spectra would be the same. The broadening in the feature around $\omega=\mu$, with increasing T is obvious. While the width itself requires a numerical estimate (which we do next) note that the height $A_{\uparrow}(0)$ first falls with increasing T and then weakly rises past T_c . Panel (b) shows the result at a non polaronic point, again J'=2t but at n=7.5%. Here the amplitude $A_{\uparrow}(0)$ decreaes monotonically with T and the width visibly increases.

Fig.12 shows the broadening Γ_{\uparrow} , indicative of the scattering rate, as a function of temperature. The red symbols correspond to the polaronic parameter point, the blue to the non polaronic. Γ_{\uparrow} in the non polaronic case is monotonically increasing, while in the polaronic case it has a peak near T_c and falls to a value characteristic of the J' value. Compare this with the T dependence of $\epsilon_c - \mu$ in Fig.10, where ϵ_c approaches μ and again draws away as T goes past T_c .

This shows that a polaronic phase can have a spontaneous density inhomogeneity but the states near μ need not be lo-

calised for an anomaly to be seen in the scattering rate and resistivity. This is more subtle than a 'strong localisation' scenario (which anyway does not happen without a pinning disorder, where a mobility gap appears in the density of states and one gets activated transport in the paramagnetic phase.

VIII. CONCLUSION

In this paper, we have established the regime in electron-spin coupling J' and density n over which magnetic polarons can exist in the ferromagnetic Heisenberg-Kondo lattice model. We find that polarons exist only above a critical coupling $J' \sim 0.7t$, and no polarons are possible for density $n \gtrsim 5\%$, however large the coupling. The polaronic phase exists when $J' > J_c'(n)$. The temperature window around T_c over which polaronic effects are seen shrinks as J' reduces towards $J_c'(n)$, and saturates for $J' \gg J_c'(n)$. We find that in the non polaronic regime the resistivity $\rho(T,J',n)$ is reasonably described by a form $(1/n)J'^2/(1+J'^2)f(T/T_c)$, all the way from weak to strong coupling, where the function f rises from zero at T=0 and saturates for $T\gg T_c$. The polaronic phase, by contrast, shows an 'excess resistivity' beyond this background, with a peak near T_c . To trace its origin, we

examined the inverse participation ratio (IPR) of electronic states in the equilibrium magnetic backgrounds at different temperatures. We find that in the non polaronic regime all states are extended at all temperatures, while for a parameter point in the polaronic window a fraction of states below the chemical potential get localised as temperature rises towards T_c . This fraction rises as $T \rightarrow T_c$ and falls again as T increases beyond T_c . Typically, except at very low n, the mobility edge only approaches the chemical potential as $T \to T_c$ but does not cross. In this situation, the transport would be determined by a scattering rate that is enhanced beyond the naive perturbative value for $T \to T_c$ and falls thereafter. To check this possibility, we calculated the electronic spectral function $A_{\sigma}(\mathbf{k},\omega)$ and probed the quasiparticle scattering rate as a function of temperature. It indeed shows a non monotonicity in the polaronic regime and mimics the monotonic resistivity in the non polaronic window. On the whole, we find that a low density strong coupling electron-spin system can display spontaneous density inhomogeneities but not strong localisation. The anomalies in resistivity arise from enhanced scattering due to proximity to a mobility edge, rather than genuine localisation and a gap in the spectrum.

Acknowledgment: We acknowledge use of the HPC clusters at HRI.

- [1] S. von Molnar and S. Methfessel, J. Appl. Phys. 38, 959 (1967).
- [2] M. F. Hundley, M. Hawley, R. H. Heffner, Q. X. Jia, J. J. Neumeier, J. Tesmer, J. D. Thompson, X. D. Wu; Transport-magnetism correlations in the ferromagnetic oxide $La_{0.7}Ca_{0.3}MnO_3$. Appl. Phys. Lett. 7 August 1995; 67 (6): 860–862 (1995).
- [3] P. Nyhus, S. Yoon, M. Kauffman, S. L. Cooper, Z. Fisk, and J. Sarrao, Spectroscopic study of bound magnetic polaron formation and the metal-semiconductor transition in EuB6, Phys. Rev. B 56, 2717 (1997).
- [4] A. P. Ramirez, M. A. Subramanian, Large Enhancement of Magnetoresistance in Tl₂Mn₂O₇: Pyrochlore Versus Perovskite, Science 277, 5325 (1997).
- [5] Moln´r, S.v. Static and Dynamic Properties of the Insulator–Metal Transition in Magnetic Semiconductors, Including the Perovskites. Journal of Superconductivity 14, 199–204 (2001).
- [6] M Ziese, Extrinsic magnetotransport phenomena in ferromagnetic oxides, Rep. Prog. Phys. 65 143 (2002).
- [7] M Ziese, Extrinsic magnetotransport phenomena in ferromagnetic oxides, Rep. Prog. Phys. 65 143 (2002).
- [8] Z. Yang, X. Bao, S. Tan, and Y. Zhang, Magnetic polaron conduction in the colossal magnetoresistance material Fe_{1-x}Cd_xCr₂S₄, Phys. Rev. B 69, 144407 (2004).
- [9] M. L. Brooks, T. Lancaster, S. J. Blundell, W. Hayes, F. L. Pratt, and Z. Fisk, Magnetic phase separation in EuB6 detected by muon spin rotation, Phys. Rev. B 70, 020401(R) (2004).
- [10] S. Kimura, T. Ito, H. Miyazaki, T. Mizuno, Takuya Iizuka, and T. Takahashi, Electronic inhomogeneity *EuO*: Possibility of magnetic polaron states Phys. Rev. B 78, 052409 (2008).
- [11] P. Das, A. Amyan, J. Brandenburg, J. Müller, P. Xiong, S. von Molnár, and Z. Fisk, Magnetically driven electronic phase separation in the semimetallic ferromagnet EuB6, Phys. Rev. B 86,

- 184425 (2012).
- [12] C. Lin, C. Yi, Y. Shi, L. Zhang, G. Zhang, Jens Müller, and Y. Li, Spin correlations and colossal magnetoresistance in HgCr2Se4, Phys. Rev. B 94, 224404 (2016).
- [13] M. Pohlit, S. Rößler, Y. Ohno, H. Ohno, S. von Molnár, Z. Fisk, J. Müller, and S. Wirth, Evidence for Ferromagnetic Clusters in the Colossal-Magnetoresistance Material EuB6, Phys. Rev. Lett. 120, 257201 (2018).
- [14] R. R. Heikes and C. W. Chen, Evidence for impurity bands in La-doped EuS, Physics Physique Fizika 1, 159 (1964).
- [15] Y. Shapira, S. Foner, and T. B. Reed, Resistivity and Hall Effect in Fields up to 150 kOe, Phys. Rev. B 8, 2299 (1973).
- [16] S. Paschen, D. Pushin, M. Schlatter, P. Vonlanthen, H. R. Ott, D. P. Young, and Z. Fisk, Electronic transport in $Eu_{1-x}Ca_xB_6$, Phys. Rev. B **61**, 4174 (2000).
- [17] Li, H., Xiao, Y., Schmitz, B. et al. Possible magnetic-polaronswitched positive and negative magnetoresistance in the GdSi single crystals. Sci Rep 2, 750 (2012).
- [18] F. Leuenberger, A. Parge, W. Felsch, K. Fauth, and M. Hessler, GdN thin films: Bulk and local electronic and magnetic properties, *Phys. Rev. B* 72, 014427 (2005).
- [19] Michael E. Fisher and J. S. Langer. Resistive Anomalies at Magnetic Critical Points, Phys. Rev. Lett. 20, 665 (1968).
- [20] P. Majumdar and P. Littlewood, Magnetoresistance in Mn Pyrochlore: Electrical Transport in a Low Carrier Density Ferromagnet, Phys. Rev. Lett. 81, 1314 (1998).
- [21] M. J. Calderón, L. Brey, and P. B. Littlewood, Stability and dynamics of free magnetic polarons, Phys. Rev. B 62, 3368 (2000).
- [22] Tao Liu, Mang Feng, Kelin Wang, A variational study of the self-trapped magnetic polaron formation in double-exchange model, Physics Letters A, Volume 337, Issues 4–6, 2005.

- [23] L. Craco, C. I. Ventura, A. N. Yaresko, and E. Müller-Hartmann, Mott-Hubbard quantum criticality in paramagnetic CMR pyrochlores, Phys. Rev. B 73, 094432 (2006).
- [24] M. J. Calderón, L. G. L. Wegener, and P. B. Littlewood, Evaluation of evidence for magnetic polarons in EuB6, Phys. Rev. B 70, 092408 (2004).
- [25] L. G. L. Wegener and P. B. Littlewood, Fluctuation-induced hopping and spin-polaron transport, Phys. Rev. B 66, 224402 (2002).
- [26] J. Chatterjee, U. Yu, and B. I. Min, Spin-polaron model: Transport properties of EuB6, Phys. Rev. B 69, 134423 (2004).
- [27] U. Yu and B. I. Min, Magnetic and Transport Properties of the Magnetic Polaron: Application to Eu_{1-x}La_xB₆ System, Phys. Rev. Lett. **94**, 117202 (2005).
- [28] U. Yu and B. I. Min, Magnetic-phase transition in the magnetic-polaron system studied with the Monte Carlo method: Anomalous specific heat of EuB6, Phys. Rev. B 74, 094413 (2006)
- [29] Tanmoy Mondal, Pinaki Majumdar, Inhomogeneous tunneling, nonmonotonic resistivity, and non-Drude optics in EuB₆, Phys. Rev. B 111, 195103 (2025).
- [30] Prüser, H., Dargel, P., Bouhassoune, M. et al. Interplay between the Kondo effect and the Ruderman–Kittel–Kasuya–Yosida interaction. Nat Commun 5, 5417 (2014)
- [31] S.J. Yamamoto, and Q. Si, Metallic ferromagnetism in the Kondo lattice, Proc. Natl. Acad. Sci. U.S.A. 107 (36) 15704-15707.
- [32] G. R. Stewart, Heavy-fermion systems, Rev. Mod. Phys. 56, 755 Published 1 October, (1984).

- [33] N. Metropolis, A. W. Rosenbluth, M. N. Rosenbluth, A. H. Teller, E. Teller, Equation of State Calculations by Fast Computing Machines, J. Chem. Phys. 21, 1087–1092 (1953).
- [34] Pui-Wai Ma and S. L. Dudarev, Langevin spin dynamics, Phys. Rev. B 83, 134418 (2011).
- [35] P.-W. Ma and S. L. Dudarev, Phys. Rev. B 86, 054416 (2012).
- [36] Gia-Wei Chern, Kipton Barros, Zhentao Wang, Hidemaro Suwa, and Cristian D. Batista, Semiclassical dynamics of spin density waves, Phys. Rev. B 97, 035120 (2018).
- [37] Cengiz Şen, Gonzalo Alvarez, Horacio Aliaga, and Elbio Dagotto, Colossal magnetoresistance observed in Monte Carlo simulations of the one- and two-orbital models for manganites, Phys. Rev. B 73, 224441 (2006).
- [38] Cengiz Şen, Gonzalo Alvarez, and Elbio Dagotto, Competing Ferromagnetic and Charge-Ordered States in Models for Manganites: The Origin of the Colossal Magnetoresistance Effect, Phys. Rev. Lett. 98, 127202 (2007).
- [39] K. Binder and D. P. Landau, Critical properties of the twodimensional anisotropic Heisenberg model, Phys. Rev. B 13, 1140 (1976).
- [40] E. M. Kogan and M. I. Auslender, Theory of the double-exchange model with arbitrary Hund coupling, Phys. Status Solidi B 147, 613 (1988).
- [41] C. M. Varma, Electronic and magnetic states in the giant magnetoresistive compounds, Phys. Rev. B 54, 7328 (1996).